

Impact of Fluid-Rock Interaction on Strength and Hydraulic Transmissivity Evolution in Shear Fractures Under Hydrothermal Conditions

Tamara Jeppson and David Lockner

U.S. Geological Survey, Earthquake Science Center, 345 Middlefield Rd. MS977, Menlo Park, CA 94025

tjeppson@usgs.gov

Keywords: Fluid-rock interactions, shear fractures, frictional healing, sealing, hydraulic transmissivity

ABSTRACT

Reactivated shear fractures contribute to the creation of pervasive fracture networks in geothermal systems. The creation, reactivation, and sustainability of fracture networks depend on complex coupling among thermal, hydraulic, mechanical, and chemical (THMC) processes. However, most laboratory experiments focus either solely on how fluid transport properties evolve in stationary fractures at elevated temperatures or on how strength evolves in shear faults at room temperature. Studies that examine the combined evolution of these properties, especially under hydrothermal conditions, are limited. Laboratory restrengthening tests, referred to as slide-hold-slide (SHS), measure the difference between the steady sliding strength and the peak shear strength immediately following a hold period at constant stress or displacement. We present the results of five SHS experiments on Westerly granite bare surfaces. These experiments are combined with in-plane flow tests and conducted at an effective confining pressure of 20 MPa and temperatures of 23 and 200 °C. Consistent with previous studies, we observe a greater reduction in fluid transmissivity at 200 °C than at 23 °C and, generally, strength increasing with log(hold duration). However, there are deviations from the expected frictional healing behavior that likely relate to mineralogy and pore fluid chemical equilibrium. For example, under no-flow conditions where fluid is allowed to equilibrate with the rock, restrengthening rate of coefficient of friction is initially 0.02 per decade change in hold time (decade⁻¹) for holds $\leq 5 \times 10^4$ s. Contrary to expected behavior, time-dependent reduction in frictional healing occurs at a rate of -0.03 decade⁻¹ for holds longer than 5×10^4 s. For flow-through tests in which undersaturated fluid is continuously introduced to the fault surface, this reduction begins earlier, starting at 5×10^3 s, but at the same rate of -0.03 decade⁻¹. The earlier onset of reduction in frictional healing under the continuous flow conditions suggests that the process underlying the behavior is related to chemical equilibrium. The mechanisms behind the complex healing behavior are not fully understood but it is apparent that fault zone restrengthening under hydrothermal conditions is the result of multiple interacting processes.

1. INTRODUCTION

Healing in fracture networks at hydrothermal conditions is a complex process resulting from coupled thermal, hydraulic, mechanical, and chemical (THMC) mechanisms. As viability and longevity of enhanced geothermal systems is dependent on the creation, reactivation, and sustainability of open fracture networks there is a critical need to improve our understanding of the healing process. Currently the interactions among THMC processes in fractures are not well constrained.

In slide-hold-slide (SHS) experiments intervals of shearing are separated by quasi-static hold periods. These tests provide a simple analog for the seismic cycle (induced or naturally occurring) with the slip and hold periods representing coseismic and interseismic periods. In these tests, the static, or peak, friction increases with the hold duration (Dieterich, 1972). Combining SHS experiments with in-plane flow tests enables an examination of the evolution of fluid transport properties and strength with time and slip. Such studies are rare. In tests on bare surface granite at room temperature no significant changes in the fluid transport or frictional properties were observed for holds lasting up to 20 days (Kishida et al., 2011). Olsen et al. (1998) examined restrengthening and sealing, defined as the overall permeability reduction, in simulated gouge composed of a mixture of quartz and labradorite at geothermal conditions. There was an overall loss of permeability over the course of the experiment, thought to be caused by secondary mineral precipitation, although permeability recovered to some extent during intervals of sliding. Olsen et al. (1998) did not observe clear static friction peaks upon reactivation of the fracture surface.

To elucidate how THMC processes affect fractures in geothermal reservoirs, we have carried out SHS experiments on simulated fractures in Westerly granite under fluid-saturated conditions at an effective confining pressure of 20 MPa and temperatures of 23° and 200 °C (Jeppson & Lockner, 2022). This experimental work examines the evolution of fluid transport properties and strength as a function of time and temperature.

2. METHODS

Frictional sliding experiments were performed in the conventional triaxial configuration on 2.54-cm diameter by ~6.1 cm long cylindrical samples of Westerly granite cut by a sawcut inclined at 30° from vertical. Sawcut surfaces were ground flat and roughened using #240 silica carbide abrasive powder producing a root-mean-square (RMS) roughness of 4 to 5 μm . Offset 4.8 mm-diameter boreholes were drilled into samples to provide fluid access to the surface (Figure 1). A 6 to 7 mm long groove was scribed on the sawcut surface, intersecting the borehole perpendicular to the long axis of each sawcut surface, to facilitate near-parallel flow across the surface between

the boreholes. Actual flow paths are longer than parallel flow paths. Numerical calculations of steady flow using the actual fault surface geometry indicate an approximately 30% reduction in flow resistance compared to idealized parallel flow between the scribed grooves (and therefore a 30% reduction in calculated transmissivity).

Samples were inserted in lead tubes with 1.0 mm wall thickness. Two viton O-rings located near each end of the jacket provided seals to isolate the sample and pore fluid from argon gas used to apply confining pressure. The sample assembly was placed in the furnace and loaded into the pressure vessel as is illustrated in Figure 1. A thermocouple was placed in the borehole at the top of the upper sample half to monitor temperature. A greased Teflon shim, placed between the sample assembly and the forcing piston, accommodates lateral slip of the lower half of the sample during shear. The sample and pore pressure system were evacuated before applying confining pressure and introducing pore fluid (deionized water).

Experiments were conducted at 30 ± 0.03 MPa constant confining pressure with 10 ± 0.0009 MPa pore pressure (deionized water). An external load cell was used to measure the axial load with a precision of 2 MPa. Two tests were conducted at a temperature of 23 °C and three were at 200 °C. Temperature was raised to 200 °C over a period of 40 to 60 minutes after the target pressure condition had been reached. The sawcut was positioned in the center of the furnace so that temperatures reported here refer to the maximum temperature in the center of the surface. In the 200 °C runs, temperature at the ends of the sawcut are 3.4% lower. During an experiment the temperature typically was maintained to within ± 0.5 °C with occasional fluctuations of up to ± 2 °C.

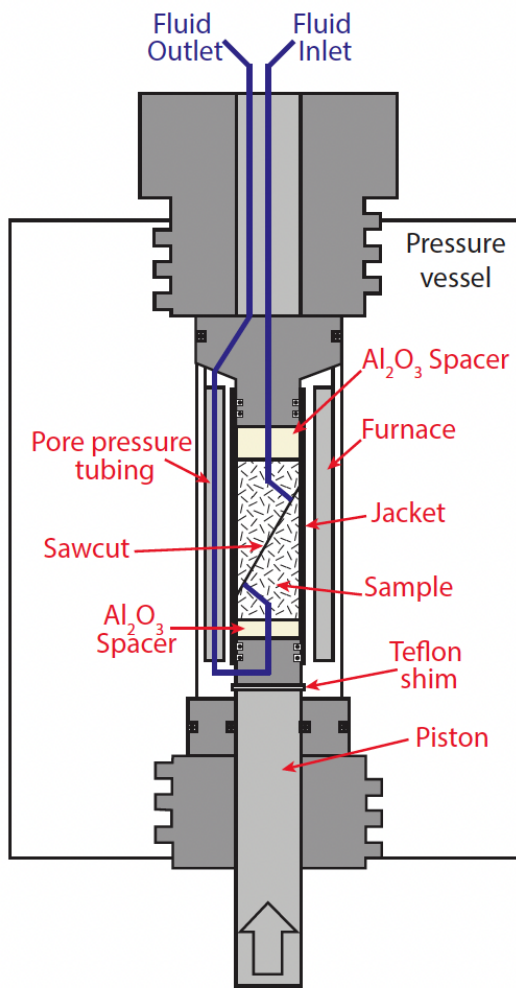


Figure 1. Schematic of the triaxial apparatus and sample geometry used in this study.

We begin each experiment with an initial 1 mm run-in before starting the first hold period. Each hold has a specified duration (t_h) followed by 0.25 mm of axial displacement at a rate of 0.1 $\mu\text{m/s}$. Axial displacement (measured on the piston outside of the pressure vessel) was corrected for the elastic deformation of the loading system and inclined fault geometry to calculate the slip resolved on the sawcut, assuming all permanent sample shortening was due to slip. Real time corrections for seal friction and changes in cross-sectional area due to slip (Scott et al., 1994; Tembe et al., 2010) were applied when calculating the stress during the experiment. Additionally, we applied a correction for jacket strength; as lead has a low strength, high ductility, and little strain hardening these corrections are small (Moore & Lockner, 2008, 2011). For the 1 mm wall jackets, yield stress, expressed as a correction to shear stress resolved on the fault, is 0.94 MPa

at 23°C decreasing to 0.21 MPa at 200 °C. Most importantly for these experiments, the lead jackets deform plastically so shear stress peaks observed upon re-initiation of slip are not jacket artifacts.

Three fluid flow conditions were used in this study: (1) no flow, (2) cycled flow, and (3) continuous flow. In the **no flow condition**, the sample was saturated and a constant pore pressure of 10 MPa was applied throughout the experiment. In these tests, a 24+ hour equilibration period preceded the initial run-in period of slip on the sawcut surface to allow the pore fluid to approach chemical equilibrium with the rock. For the **cycled flow conditions**, a 2 MPa pore pressure differential was applied, and a set volume of fluid (~ 1.5 ml) flowed along the sawcut and discharged into a reservoir on the low side. The flow direction was then reversed and the process repeated so that the same volume of pore fluid was regularly cycled along the simulated fault. The fluid was cycled during an initial 24+ hour equilibration period and throughout the experiment. In the **continuous flow case**, after saturating the sample a pore pressure differential of 2 MPa was applied between the injection boreholes in the simulated fault (11 MPa at the top and 9 MPa at the bottom) so that fluid flow was always in the same direction. These tests did not incorporate an equilibration period at temperature. Rather, deionized water was continuously introduced to the sawcut and flushed from the system.

For the continuous and cycled flow conditions, flow rate and pressure drop were measured during the experiments. For a fracture-dominated system, the measured flow rate is affected by the fracture aperture which we do not measure directly. For this reason, we report hydraulic transmissivity (κ) of the fracture, which we define as the product of permeability (k) and fracture aperture (a). This definition of hydraulic transmissivity is commonly used to describe a fracture's fluid transport properties when the aperture is unknown (Zimmerman & Bodvarsson, 1996; Rutter & Mecklenburgh, 2017, 2018). It is related to the more commonly defined hydraulic transmissivity, κ_K (defined as the product of hydraulic conductivity and aperture) according to

$$\kappa = ka = \frac{v_f Q L}{w \Delta P} = \frac{\kappa_K v_f}{\rho g} \quad (1)$$

where v_f is the dynamic viscosity of water (0.136 cP at 200 °C), ρ is the fluid density, g is gravitational acceleration, Q is the volumetric flow rate, L is the distance between the boreholes, w is the length of the groove scribed on the sawcut surface, and ΔP is the pore pressure differential. This definition assumes non-divergent steady flow. Given the geometry of the fault surfaces, average width of the flow path between boreholes is larger than w and true transmissivity is about 30% less than the values reported here. Flow rate is measured at the pore pressure pump, which is at room temperature, based on volume change with time in the down stream pump. Assuming conservation of fluid mass, the flow rate through the sample at elevated temperature is:

$$Q_{200\text{ }^{\circ}\text{C}} = Q_{23\text{ }^{\circ}\text{C}} \left(\frac{V_{200\text{ }^{\circ}\text{C}}}{V_{23\text{ }^{\circ}\text{C}}} \right) \quad (2)$$

Where V is the specific volume of water ($V_{200\text{ }^{\circ}\text{C}} = 0.0011 \text{ m}^3/\text{kg}$ at 20 MPa) and the subscript denotes the temperature in degrees Celsius. Typical errors in the hydraulic conductivity are $\pm 3.5\%$ and the lower limit for transmissivity is $1 \times 10^{-22} \text{ m}^3$. We calculated transmissivity for 15-minute intervals of flow.

3. RESULTS

3.1 Steady-state sliding

The sawcut surface undergoes strain hardening over the entire course of each experiment (Figure 2). This behavior is likely due to continued evolution of the shear surface via the generation, comminution, and compaction of wear products. We use the general trend of the strain hardening behavior to determine the steady-state sliding friction, defined as ratio of shear stress to effective normal stress ($\mu = \tau / \sigma_{\text{Neff}}$). At room temperature the steady state friction increases from 0.62 at 0.93 mm to 0.84 at 4.6 mm of shear displacement (Figure 2a).

At 200 °C it can be difficult to maintain steady-state sliding on the sawcut surface, because the samples tend toward unstable slip as displacement increases. This instability results in oscillations in the sliding friction. Where stable sliding is observed, the steady-state coefficient of friction ranges from 0.60 to 0.78. The minimum value is observed at ~1 mm of shear displacement increasing with continued shearing. Following Jeppson et al. (2021), we estimate steady-state friction in the unstable portions based on the magnitude and recurrence interval of the small stick-slip events that occur while sliding and the restrengthening model proposed by Nakatani & Scholz (2004). The estimated steady-state friction reaches a maximum of 0.87 after 6.2 mm of shear displacement.

3.2 Frictional healing

Hold durations in these experiments ranged from 1×10^2 to 5×10^5 s. As the sample is reloaded following the hold period, the friction increases until a peak value is reached and the sample begins to slide. The friction then decreases and, as sliding continues, returns to the steady-state sliding condition. Conventionally, the difference between this peak friction and the steady-state friction of the preceding slide defines the magnitude of frictional healing during the hold period ($\Delta\mu = \mu_p - \mu_{ss}$). At room temperature, peak friction following the hold is always equal to or greater than the steady-state sliding friction (Figure 2a). The magnitude of these peaks increases with hold duration at a rate of 0.009 ± 0.004 per decade change in hold time (decade⁻¹) (Figure 3).

The hydrothermal experiments are more complex. Over short hold periods ($\leq 5 \times 10^3$ s) the behavior is similar to the room temperature test, with peaks in friction following hold periods that are greater than the steady-state sliding friction. Over these short holds, time-dependent frictional healing increases at a rate of 0.013 ± 0.005 decade $^{-1}$. However, for longer hold periods we observe a reduction in frictional healing with time. In the no flow tests, peak friction has a negative dependence on time for holds longer than 5×10^4 s (Figure 4a). The peak friction of these long holds is often followed by a large stress drop and rapid strain hardening as the sliding friction returns to steady state. Similar behavior is observed in the cycled flow test for hold durations between 5×10^4 and 5×10^5 s but the behavior following the 5×10^5 s hold is different. Following the 5×10^5 s hold in the cycled test, the peak friction does not exceed the steady-state friction of the preceding slide (Figure 4b), resulting in negative values of $\Delta\mu$. These peaks are not followed by large stress drops but there is significant strain hardening. However, the amount of displacement required to return to the previous strain hardening trend that we used to define steady-state sliding exceeds 0.2 mm. The same behavior is observed for hold durations $> 1 \times 10^4$ s in the continuous flow test. The overall rate of frictional healing for the longer holds is -0.044 ± 0.023 decade $^{-1}$.

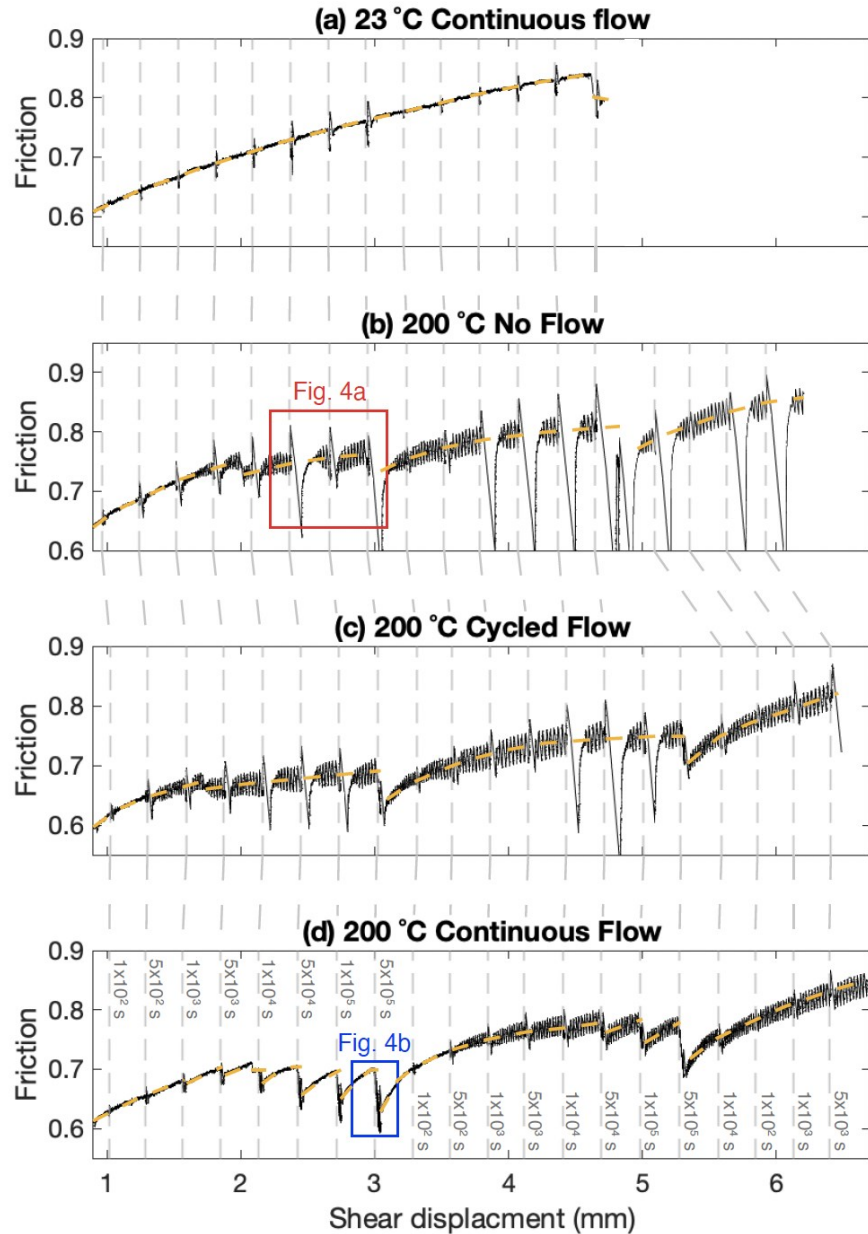


Figure 2. Evolution of coefficient of friction with displacement resolved on the fault surface for selected experiments at (a) 23 °C with continuous flow, (b) 200 °C with no flow, (c) 200 °C with cycled flow, and (d) 200 °C with continuous flow (Jeppson & Lockner, 2022). Holds ranged from 1×10^2 to 5×10^5 s; locations of holds are indicated by the gray dashed lines. Experiments at 200 °C tend to slip unstably, leading to oscillations in the sliding shear stress. The estimated steady-state sliding friction is indicated by the dashed yellow line. Red and blue boxes indicate the locations of figures 4a and 4b, respectively. All runs were at 20 MPa effective confining pressure.

The clear presence of a peak friction associated with the long hold durations suggests there is strengthening relative to the short-term steady-state friction following the hold. But this peak friction is dramatically lower than the prior steady-state level and also the long term trend of steady-state friction suggesting weakening at the same time. Low sliding friction and long characteristic slip distance following these holds may indicate that the friction properties of the sawcut surface and thin gouge layer are evolving during the hold to have a different steady-state sliding friction. If we define the new steady-state sliding friction based on the strain hardening trend of the slide following the hold and set $\Delta\mu'$ to be the difference between this new steady-state friction and the peak friction (Figure 4b) then $\Delta\mu'$ is always positive and we observe a time-dependent increase in frictional healing at a rate of 0.008 decade⁻¹ (Figure 3).

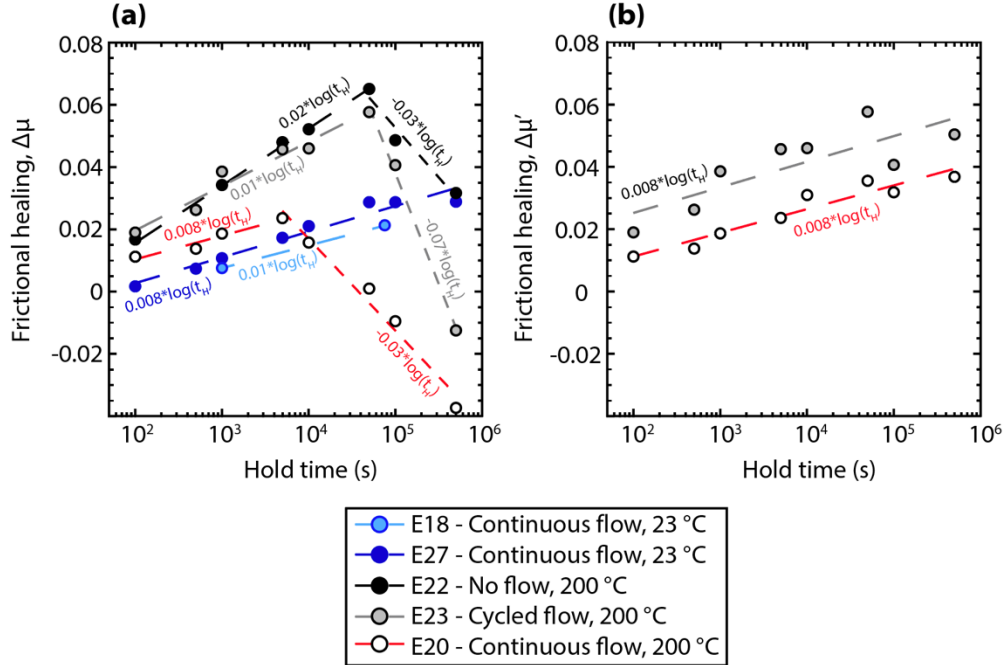


Figure 3. Average frictional healing plotted relative to hold time. (a) Average frictional healing ($\Delta\mu$), defined relative to the sliding friction of the preceding slide, exhibits a transition from a positive to negative dependence on time at 5×10^4 s for the cycled and no flow conditions. This transition occurs an order of magnitude earlier for the continuous flow case. (b) Average frictional healing ($\Delta\mu'$), defined relative to the sliding friction of the following slide exhibits time-dependent increase in healing.

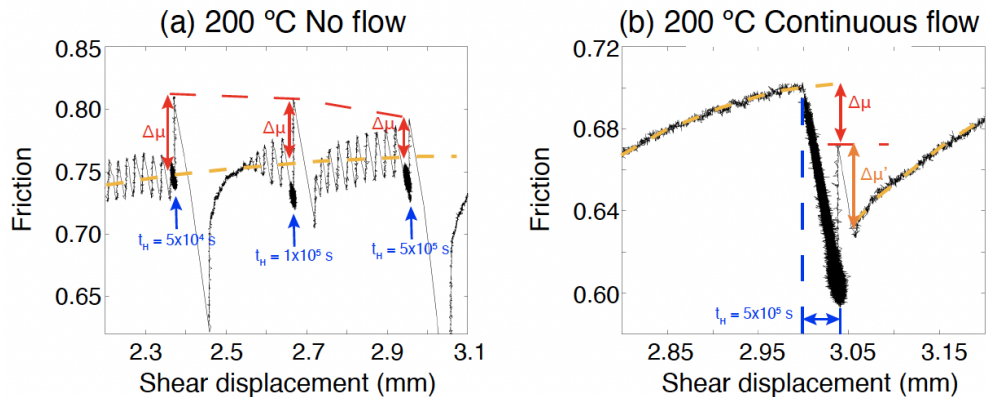


Figure 4. Evolution of coefficient of friction with displacement resolved on the fault surface for (a) hold durations of 5×10^4 to 5×10^5 s at 200 °C with no fluid flow and (b) a 5×10^5 s hold at 200 °C with continuous fluid flow (Jeppson & Lockner, 2022). Locations of the holds shown in this figure are indicated by the red and blue boxes in figure 2. The estimated steady-state friction is indicated by the dashed yellow line. $\Delta\mu$ is the difference in friction measured relative to the steady-state friction preceding the hold while $\Delta\mu'$ is relative to the steady-state friction after the hold.

3.3 Hydraulic transmissivity

Hydraulic transmissivity was calculated from the flow rate measured during cycled and continuous flow experiments. The transmissivity decreases during each experiment. At 200 °C, this reduction is basically logarithmic, occurring more rapidly early in the experiments and slowing with time (Figure 5). At 23 °C, the reduction is also rapid early but slows significantly after ~4 hours. Increases in the hydraulic conductivity occur during many of the sliding periods. The magnitude of recovery tends to increase with hold time.

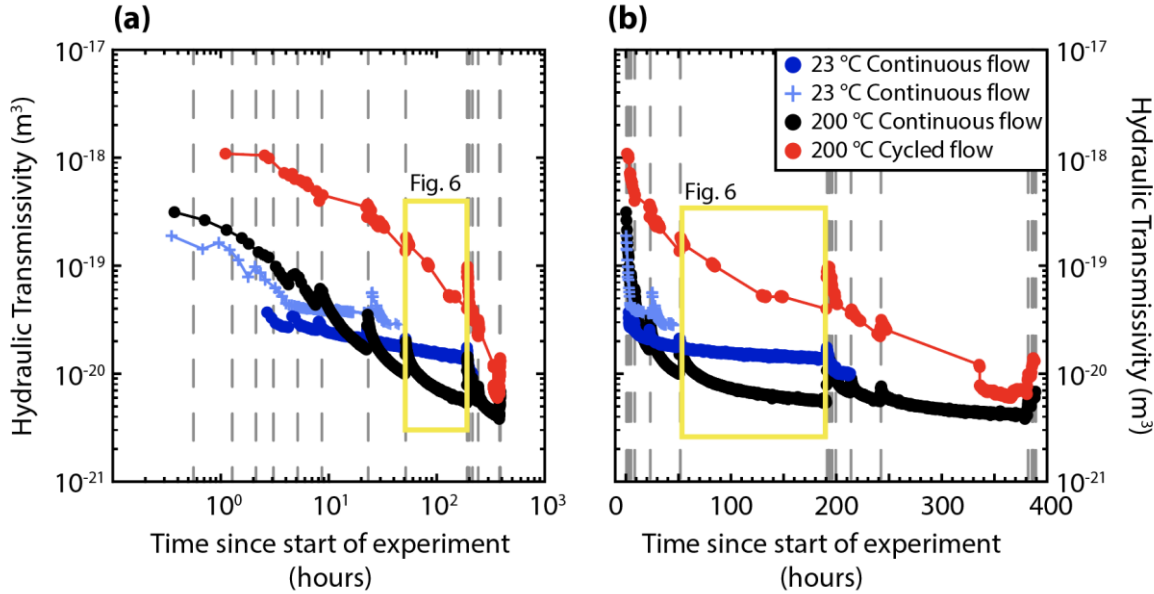


Figure 5. Evolution of hydraulic transmissivity with time shown on (a) log-log and (b) log-linear scales (Jeppson & Lockner, 2022). Time zero is set when the first slide begins. Slide periods are indicated by gray dashed lines, slides are commonly associated with increases in the transmissivity. The 5×10^5 s hold period shown in figure 6 is indicated by the yellow box.

Fluid transmissivity continuously decreases during the hold periods. Figure 6 shows the evolution of hydraulic transmissivity with time during a 5×10^5 s hold. At 23 °C there is a rapid decrease ($-1.5 \text{ m}^3/\text{decade}$) in transmissivity for the first ~6 hours after which the reduction rate decreases to $-0.3 \text{ m}^3/\text{decade}$ and there is little further change with time. Similarly, at 200 °C the reduction rate is initially fast, $-14 \text{ m}^3/\text{decade}$ and $-5 \text{ m}^3/\text{decade}$ during the first ~4 hours for the continuous and cycled flow conditions, respectively. While this rate slows with time it remains higher than was observed in the room temperature experiments, mirroring the overall trend of transmissivity during the full experiments shown in figure 5. The 200 °C experiments reach a $-0.3 \text{ m}^3/\text{decade}$ loss rate, equivalent to the rate observed in the 23 °C test, during the final 90 hours of the hold period. Fluid flow conditions appear to have little effect on transmissivity loss, although loss rate may remain high for a longer time in the cycled flow test.

4. DISCUSSION

4.1 Comparison to previous work

4.1.1 Strength and healing rates

Previous SHS experiments on initially bare surface Westerly granite have all been conducted on nominally dry samples (Beeler & Tullis, 1994; Mitchell et al., 2013; Ryan et al., 2018). These studies document a range in steady-state sliding friction from 0.65 to 0.81. This range is generally consistent with values of sliding friction found in the current study, although 0.87 (Jeppson & Lockner, 2022) is higher than expected for bare surface granite (Beeler & Tullis, 1994; Mitchell et al., 2013; Ryan et al., 2018).

In previous studies at room temperature and humidity, a log-linear growth in $\Delta\mu$ with time has been well-documented for both bare surface and gouge studies on a variety of materials (e.g., Dieterich, 1972; Dieterich & Kilgore, 1994; Karner & Marone, 2000; Carpenter et al., 2016). The rate of frictional healing in our room temperature data, acquired under saturated conditions, is slightly lower than the 0.02 decade^{-1} observed in previous studies on nominally dry, bare surface Westerly granite (Beeler & Tullis, 1994; Mitchell et al., 2013). Similar experiments at hydrothermal conditions are very limited. The only work we know of to have examined restrengthening on bare surface Westerly granite at elevated temperatures was conducted on nominally dry samples at 200 °C (Mitchell et al., 2013). That study showed no difference between tests conducted at room temperature and 200 °C. This observation is not surprising, in that solution-transfer processes, which would be more active at elevated temperatures, depend on the water phase for transfer of reactive species. Further, no reduction in frictional healing is observed at longer hold times, up to 1×10^5 s. Studies at hydrothermal conditions have predominantly focused on behavior of simulated gouge layers composed of quartz (Chester & Higgs, 1992; Karner et al., 1997; Nakatani & Scholz, 2004) or bare surface Fontainebleau sandstone (Tenthorey et al., 2003; Tenthorey & Cox, 2006), all of which were characterized by time-dependent increases in frictional healing for holds up to 3×10^5 s. The Olsen et al. (1998) study is an exception in that time-dependent healing was not observed in tests performed on water-saturated gouge layers composed of a mixture of 90% quartz and 10% labradorite

at temperatures up to 250 °C. Van der Ende & Niemeijer (2019) measured a reduction in the frictional healing rate for holds exceeding 1×10^4 s in room temperature tests on halite gouge, a rock analog used to simulate hydrothermal conditions. This reduction appears to be related to the transition from dominantly frictional healing processes to cohesive healing processes.

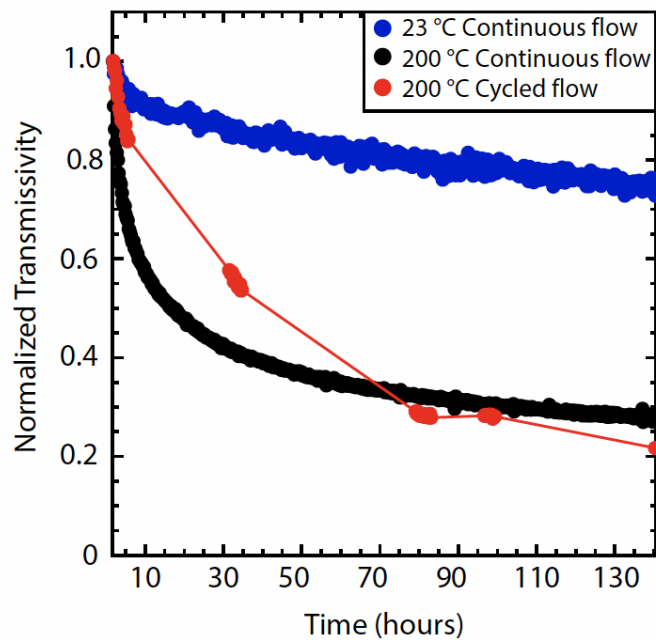


Figure 6. Hydraulic transmissivity loss with time during a 5×10^5 s hold (Jeppson & Lockner, 2022). Timings of these holds within the full experiment are indicated by the yellow boxes in figure 5. For comparison across experiments, transmissivity is normalized by the transmissivity at the start of the hold period.

4.1.2 Fluid transport properties

Many previous experimental studies have examined the effects of shearing on fluid transport properties in fractures. Most of these have been conducted at room temperature (e.g., Zhang & Tullis, 1998; Yeo et al., 1999; Zhang et al., 1999; Kishida et al., 2011; Im et al., 2018, 2019; Rutter & Mecklenburgh, 2018), and they showed an initial rapid loss in hydraulic transmissivity upon initiation of shearing. These rapid reductions were attributed to development of the shear surface through the generation of wear products, compaction, and comminution (Zhang & Tullis, 1998; Zhang et al., 1999). Subsequent sliding then led to increases in hydraulic transmissivity due to shear dilation (Zhang et al., 1999; Im et al., 2019). All studies reported continuous transmissivity reduction during hold periods due to compaction.

At hydrothermal conditions, the rate of transmissivity reduction increases with increasing temperature in both stationary (Moore et al., 1994; Morrow et al., 2001) and sheared (Olsen et al., 1998; Tenthorey et al., 2003) fractures. The increased transmissivity reduction at hydrothermal conditions relative to room temperature indicates that the difference is due to a thermally activated process that is occurring more rapidly at higher temperatures (Moore et al., 1994; Morrow et al., 2001).

4.2 Potential mechanisms

Under room temperature conditions the possible mechanisms behind the observed restrengthening are limited in number. The primary mechanism is expected to be increases in the contact area (Dieterich & Kilgore, 1994) via compaction and densification (Ryan et al., 2018), indentation creep (Scholz & Engelder, 1976), and subcritical crack growth (Atkinson, 1984). Other possible mechanisms include the desorption of water molecules (Westbrook & Jorgensen, 1968) and diffusion of water away from high-stress contacts (Scholz, 2019).

At hydrothermal conditions there is greater complexity in the processes underlying the frictional healing. Not only are the room temperature mechanisms still applicable but there is also the potential for additional thermal and chemical processes. Processes such as pressure solution may be active at room temperature but would occur more rapidly at higher temperatures and thus be more likely to be observed at laboratory time scales (Yasuhara et al., 2005; Niemeijer et al., 2008). In the experiments presented in this paper, the reduction in frictional healing at long hold times only occurs in the 200 °C experiments. This indicates that the underlying process is thermally activated. While previous tests on nominally dry bare surface Westerly granite yielded a continuous increase in healing rate with hold time (Beeler & Tullis, 1994; Mitchell et al., 2013), the decline in healing rate at long hold times in our hydrothermal experiments may indicate a solution transfer process. We speculate that thermally activated chemical reactions between the pore fluid and rock lead to the development of alteration products, such as phyllosilicates, that have lower strength than the host rock. Olsen et al. (1998) identified

secondary minerals precipitated in samples of labradorite + quartz gouge that had been deformed at hydrothermal conditions with cycled flow. Moore et al. (1994) found widespread evidence of mineral dissolution and precipitation on a fracture surface in Westerly granite at temperatures ≥ 300 °C. This is a reasonable hypothesis to explain the behavior of the cycled and no-flow tests. However, in the continuous flow test the pore fluid is continuously being flushed out of the system resulting in a constant removal of the dissolved ions in the discharged fluids. It is unlikely that under these conditions the pore fluid will become supersaturated with any mineral species while in the sample. We suggest that the continuous flow-through configuration may favor continued dissolution and leaching of the rock over mineral precipitation. The reduction in restrengthening may therefore be a result of preferential dissolution of mechanically strong minerals and/or leached material that is weaker than the original minerals. The rate of dissolution would be faster when the degree of chemical disequilibrium between the pore fluid and rock is higher and would slow as the system approaches chemical equilibrium (Aharonov et al., 1998; Tenthorey et al., 1998). This may explain the earlier onset of the reduction in frictional healing observed in the continuous flow test where we expect greater chemical disequilibrium.

5. CONCLUSIONS

We have presented the results of SHS experiments on water saturated, initially bare surfaces samples of Westerly granite at temperatures of 23 and 200 °C (Jeppson & Lockner, 2022). The room-temperature samples show time-dependent increases in frictional healing, consistent with previous experiments on nominally dry samples of Westerly granite. At 200 °C the restrengthening behavior is more complex. There is a positive correlation between hold time and healing for hold times $\leq 1 \times 10^3$ s, consistent with many previous hydrothermal studies, but for hold durations $\geq 5 \times 10^3$ s a negative dependence of restrengthening on time is observed. The transition from positive to negative dependence is delayed by 4.5×10^4 s for the cycled and no fluid flow test conditions relative to continuous flow. This negative dependence has not been reported in previous studies, most of which were conducted on monomineralic samples. This reduction in restrengthening may be caused by a thermally-activated solution transfer process that occurs more rapidly when there is a greater degree of chemical disequilibrium between the fluid and the rock. Although the mechanisms behind the complex healing behavior are not fully understood, it is apparent that fault zone restrengthening under hydrothermal conditions is the result of multiple interacting processes.

DISCLAIMER

Any use of trade, firm, or product names is for descriptive purposes only and does not imply endorsement by the U.S. Government.

REFERENCES

Aharonov, E., Tenthorey, E., and Scholz, C. H.: Precipitation sealing and diagenesis: 2. Theoretical analysis. *Journal of Geophysical Research: Solid Earth*, 103(B10), (1998), 23969-23981.

Atkinson, B.K.: Subcritical crack growth in geological materials. *Journal of Geophysical Research: Solid Earth*, 89(B6), (1984), 4077-4114.

Beeler, N.M., Tullis, T.E., and Weeks, J.D.: The roles of time and displacement in the evolution effect in rock friction. *Geophysical Research Letters*, 21(18), (1994), 1987-1990.

Carpenter, B.M., Collettini, C., Viti, C., and Cavallo, A.: The influence of normal stress and sliding velocity on the frictional behaviour of calcite at room temperature: insights from laboratory experiments and microstructural observations. *Geophysical Journal International*, 205(1), (2016), 548-561.

Chester, F.M., and Higgs, N.G.: Multimechanism friction constitutive model for ultrafine quartz gouge at hypocentral conditions. *Journal of Geophysical Research: Solid Earth*, 97(B2), (1992), 1859-1870.

Dieterich, J.H.: Time-dependent friction in rocks. *Journal of Geophysical Research*, 77(20), (1972), 3690-3697.

Dieterich, J.H., & Kilgore, B. D.: Direct observation of frictional contacts: New insights for state-dependent properties. *Pure and Applied Geophysics*, 143(1), (1994), 283-302.

Im, K., Elsworth, D., and Fang, Y.: The influence of preslip sealing on the permeability evolution of fractures and faults. *Geophysical Research Letters*, 45(1), (2018), 166-175.

Im, K., Elsworth, D., and Wang, C.: Cyclic permeability evolution during repose then reactivation of fractures and faults. *Journal of Geophysical Research: Solid Earth*, 124(5), (2019), 4492-4506.

Jeppson, T., and Lockner, D.: Geothermal slide-hold-slide experiments on bare surface Westerly granite. U.S. Geological Survey data release, accessed January 19, 2022, at <https://doi.org/10.5066/P9HX2EL8>.

Jeppson, T.N., Lockner, D., Kilgore, B., Beeler, N., and Taron, J.: Strength recovery and sealing under hydrothermal conditions, 55th US Rock Mechanics/Geomechanics Symposium, (2021).

Karner, S.L., and Marone, C.: Effects of loading rate and normal stress on stress drop and stick-slip recurrence interval. *Geophysical Monograph-American Geophysical Union*, 120, (2000), 187-198.

Karner, S.L., Marone, C., and Evans, B.: Laboratory study of fault healing and lithification in simulated fault gouge under hydrothermal conditions. *Tectonophysics*, 277(1-3), (1997), 41-55.

Kishida, K., Kawaguchi, Y., Nakashima, S., and Yasuhara, H.: Estimation of shear strength recovery and permeability of single rock fractures in shear-hold-shear type direct shear tests. *International Journal of Rock Mechanics and Mining Sciences*, 48(5), (2011), 782-793.

Niemeijer, A., Marone, C., and Elsworth, D.: Healing of simulated fault gouges aided by pressure solution: Results from rock analogue experiments. *Journal of Geophysical Research: Solid Earth*, 113(B4), (2008).

Mitchell, E.K., Fialko, Y., and Brown, K.M.: Temperature dependence of frictional healing of Westerly granite: Experimental observations and numerical simulations. *Geochemistry, Geophysics, Geosystems*, 14(3), (2013), 567-582

Moore, D.E., and Lockner, D.A.: Talc friction in the temperature range 25–400 C: Relevance for fault-zone weakening. *Tectonophysics*, 449(1-4), (2008), 120-132.

Moore, D.E., and Lockner, D.A.: Frictional strengths of talc-serpentine and talc-quartz mixtures. *Journal of Geophysical Research: Solid Earth*, 116(B1), (2011).

Moore, D.E., Lockner, D.A., and Byerlee, J.D.: Reduction of permeability in granite at elevated temperatures. *Science*, 265(5178), (1994), 1558-1561.

Morrow, C.A., Moore, D.E., and Lockner, D.A.: Permeability reduction in granite under hydrothermal conditions. *Journal of Geophysical Research: Solid Earth*, 106(B12), (2001), 30551-30560.

Nakatani, M., and Scholz, C.H.: Frictional healing of quartz gouge under hydrothermal conditions: 1. Experimental evidence for solution transfer healing mechanism. *Journal of Geophysical Research: Solid Earth*, 109(B7), (2004).

Olsen, M.P., Scholz, C.H., and Léger, A.: Healing and sealing of a simulated fault gouge under hydrothermal conditions: Implications for fault healing. *Journal of Geophysical Research: Solid Earth*, 103(B4), (1998), 7421-7430.

Rutter, E.H., and Mecklenburgh, J.: Hydraulic conductivity of bedding-parallel cracks in shale as a function of shear and normal stress, Geological Society, London, Special Publications 454(1), (2017), 67-84.

Rutter, E.H., and Mecklenburgh, J.: Influence of normal and shear stress on the hydraulic transmissivity of thin cracks in a tight quartz sandstone, a granite, and a shale, *Journal of Geophysical Research: Solid Earth* 123(2), (2018), 1262-1285.

Ryan, K.L., Rivière, J., and Marone, C.: The role of shear stress in fault healing and frictional aging. *Journal of Geophysical Research: Solid Earth*, 123(12), (2018), 10479-10495.

Scholz, C.H.: *The Mechanics of Earthquakes and Faulting*. Cambridge University Press, (2019).

Scholz, C.H., and Engelder, J.T.: The role of asperity indentation and ploughing in rock friction—I: Asperity creep and stick-slip. In *International Journal of Rock Mechanics and Mining Sciences & Geomechanics Abstracts*, 13(5), (1976), 149-154.

Scott, D.R., Marone, C.J., and Sammis, C.G.: The apparent friction of granular fault gouge in sheared layers. *Journal of Geophysical Research: Solid Earth*, 99(B4), (1994), 7231-7246.

Tembe, S., Lockner, D.A., and Wong, T.F.: Effect of clay content and mineralogy on frictional sliding behavior of simulated gouges: Binary and ternary mixtures of quartz, illite, and montmorillonite. *Journal of Geophysical Research: Solid Earth*, 115(B3), (2010).

Tenthorey, E., and Cox, S.F.: Cohesive strengthening of fault zones during the interseismic period: An experimental study. *Journal of Geophysical Research: Solid Earth*, 111(B9), (2006).

Tenthorey, E., Cox, S.F., and Todd, H.F.: Evolution of strength recovery and permeability during fluid–rock reaction in experimental fault zones. *Earth and Planetary Science Letters*, 206(1-2), (2003), 161-172.

Tenthorey, E., Scholz, C.H., Aharonov, E., and Léger, A.: Precipitation sealing and diagenesis: 1. Experimental results. *Journal of Geophysical Research: Solid Earth*, 103(B10), (1998), 23951-23967.

van den Ende, M.P.A., and Niemeijer, A.R.: An investigation into the role of time-dependent cohesion in interseismic fault restrengthening. *Scientific reports*, 9(1), (2019), 1-11.

Westbrook, J.H., and Jorgensen, P.J.: Effects of water desorption on indentation microhardness anisotropy in minerals. *American Mineralogist: Journal of Earth and Planetary Materials*, 53(11-12), (1968), 1899-1909.

Yasuhara, H., Marone, C., and Elsworth, D.: Fault zone restrengthening and frictional healing: The role of pressure solution. *Journal of Geophysical Research: Solid Earth*, 110(B6), (2005).

Yeo, I.W., De Freitas, M.H., and Zimmerman, R.W.: Effect of shear displacement on the aperture and permeability of a rock fracture. *International journal of rock mechanics and mining sciences*, 35(8), (1998), 1051-1070.

Zhang, S., and Tullis, T.E.: The effect of fault slip on permeability and permeability anisotropy in quartz gouge. *Tectonophysics*, 295(1-2), (1998), 41-52.

Jeppson and Lockner

Zhang, S., Tullis, T.E., and Scruggs, V.J.: Permeability anisotropy and pressure dependency of permeability in experimentally sheared gouge materials. *Journal of structural geology*, 21(7), (1999), 795-806.

Zimmerman, R.W., and Bodvarsson, G.S.: Hydraulic conductivity of rock fractures. *Transport in porous media*, 23(1), (1996), 1-30.